Original Article

JCBFM

Journal of Cerebral Blood Flow & Metabolism
2020, Vol. 40(12) 2401–2415

DOI: 10.1177/0271678X19892657
journals.sagepub.com/home/jcbfm
SAGE

Mild metabolic stress is sufficient to disturb the formation of pyramidal cell ensembles during gamma oscillations

Shehabeldin Elzoheiry[1], Andrea Lewen[1], Justus Schneider[1], Martin Both[1], Dimitri Hefter[1,2], Juan Carlos Boffi[3], Jan-Oliver Hollnagel[1,*] and Oliver Kann[1,4,*]

Abstract

Disturbances of cognitive functions occur rapidly during acute metabolic stress. However, the underlying mechanisms are not fully understood. Cortical gamma oscillations (30–100 Hz) emerging from precise synaptic transmission between excitatory principal neurons and inhibitory interneurons, such as fast-spiking GABAergic basket cells, are associated with higher brain functions, like sensory perception, selective attention and memory formation. We investigated the alterations of cholinergic gamma oscillations at the level of neuronal ensembles in the CA3 region of rat hippocampal slice cultures. We combined electrophysiology, calcium imaging (CamKII.GCaMP6f) and mild metabolic stress that was induced by rotenone, a lipophilic and highly selective inhibitor of complex I in the respiratory chain of mitochondria. The detected pyramidal cell ensembles showing repetitive patterns of activity were highly sensitive to mild metabolic stress. Whereas such synchronised multicellular activity diminished, the overall activity of individual pyramidal cells was unaffected. Additionally, mild metabolic stress had no effect on the rate of action potential generation in fast-spiking neural units. However, the partial disinhibition of slow-spiking neural units suggests that disturbances of ensemble formation likely result from alterations in synaptic inhibition. Our study bridges disturbances on the (multi-)cellular and network level to putative cognitive impairment on the system level.

Keywords

Brain slice, cognition, electrophysiology, energy metabolism, widefield microscopy

Received 21 August 2019; Revised 31 October 2019; Accepted 10 November 2019

Introduction

The mammalian brain has an exceptionally high metabolic activity. In adult humans, the brain receives 15% of the cardiac output and consumes 20% of the utilised oxygen, although contributing only 2% of the total body mass.[1–3] This indicates that information processing requires high amounts of energy and might explain the exceptional vulnerability of higher brain functions to metabolic stress.[4–7] Therefore, the proper function of the brain requires adequate vascular energy substrate and oxygen supply as well as reliable ATP synthesis by mitochondria.[1,8]

Rhythmic neuronal network activity is associated with a wide range of higher cognitive functions such as reasoning, memory formation, and decision making.[9–11] In particular, gamma oscillations have

[1]Institute of Physiology and Pathophysiology, University of Heidelberg, Heidelberg, Germany
[2]RG Animal Models in Psychiatry, Clinic of Psychiatry and Psychotherapy, Central Institute of Mental Health, Mannheim, Germany
[3]Institute for Anatomy and Cell Biology, University of Heidelberg, Heidelberg, Germany
[4]Interdisciplinary Centre for Neurosciences (IZN), University of Heidelberg, Heidelberg, Germany

*These authors contributed equally to this work.

Corresponding author:
Jan-Oliver Hollnagel, Institute of Physiology and Pathophysiology, University of Heidelberg, Im Neuenheimer Feld 326, Heidelberg D-69120, Germany.
Email: jan-oliver.hollnagel@physiologie.uni-heidelberg.de

received interest due to their importance for cognition and their exquisite sensitivity to metabolic stress.[12–15] Gamma oscillations represent oscillatory activity in the frequency band of 30–100 Hz.[10,16] These oscillations are known to be associated with cognitive functions such as selective attention, memory formation and sensory perception.[8,17,18]

Previous studies revealed a positive correlation between the power of gamma oscillations and oxygen metabolism.[13,15] Additionally, oxygen consumption rates were found to be higher during gamma oscillations compared to other activity states such as asynchronous activity and sharp wave-ripples.[13,15] In the hippocampal CA3 region, where gamma oscillations can be generated intrinsically, it was shown that neuronal mitochondria are enriched with complex I subunits.[14] Furthermore, it was observed that gamma oscillations utilise the mitochondrial oxidative capacity near limit and are very sensitive to interference with mitochondrial function by inhibition of complex I.[14] These studies indicate a selective vulnerability of gamma oscillations to metabolic stress. However, understanding the link between altered gamma oscillations and impaired cognitive functions during metabolic stress requires further insight at the level of neuronal ensembles.[19,20]

Ensembles are groups of co-active neurons with repetitive patterns of activity.[21] Network oscillations support the formation of ensembles by defining precise temporal windows for synchronised activity.[10,16] Gamma oscillations emerge from fluctuating synaptic potentials mediated via perisomatic inhibition by fast-spiking interneurons.[22] Fast-spiking interneurons are believed to have a relatively high energy demand.[19] We hypothesise that mild metabolic stress disturbs the formation of neuronal ensembles, which might also provide a correlate between disturbances at the cellular level and cognitive dysfunctions upon brain insults.[20]

Mild metabolic stress in slice preparations (*in situ*) aims to mimic pathophysiological conditions, such as acute ischemia and chronic hypoperfusion, which might be responsible for the decline in cognitive functions in cardiovascular diseases and, perhaps, aging and Alzheimer's disease.[23–25] It also aims to mimic pathophysiological conditions during mitochondrial diseases.[26–28]

Here, we used organotypic hippocampal slice cultures as a model to study the effect of mild metabolic stress on gamma oscillations.[29,30] To elicit gamma oscillations, we used the muscarinic acetylcholine receptor agonist carbachol, which increases the excitability of CA3 pyramidal cells, modulates presynaptic activity of parvalbumin-positive interneurons,[31,32] and reduces the activity of dentate gyrus granule cells,[33] thereby likely relieving the feed-forward inhibition in the CA3 network.[22] This cholinergic model simulates in vivo gamma oscillations and mimicks the increase in the acetylcholine level observed during exploratory behaviour.[34] To induce mild metabolic stress, we used rotenone which inhibits complex I of the mitochondrial respiratory chain,[35] thereby interfering with ATP synthesis. We applied local field potential (LFP) recordings to verify network activity states,[36] and calcium imaging,[37–40] to monitor a large number of pyramidal cells at the same time, which enabled us to detect pyramidal cell ensembles. Furthermore, neural spike sorting was performed to identify changes in the generation of action potentials of fast-spiking and slow-spiking neural units upon metabolic stress.[41,42]

Our results show that synchronised activity is highly vulnerable to metabolic stress during gamma oscillations. Additionally, we found that partial disinhibition of pyramidal cells disturbs co-activity of neuronal ensembles. The disinhibition is most likely reflecting functional alterations in the presynaptic compartment of fast-spiking units. These results may shed light on the high vulnerability of cognitive processes during mild impairment of oxygen and substrate supply in the brain.

Materials and methods

Animal preparation

Wistar rats were purchased from Charles-River (Sulzfeld, Germany). Caring and sacrificing of the animals were performed according to the recommendations of the European directive (2010/63/EU) and the authorities of Baden-Württemberg (T96/15 and T45/18). Experiments were performed and reported in accordance with the ARRIVE guidelines.

Organotypic slice cultures

Hippocampal slice cultures were prepared as described earlier.[14,43,44] Briefly, rats were sacrificed at the age of seven to nine days. Under sterile conditions, a McIlwain tissue chopper (Mickle Laboratory Engineering Company Ltd, Guildford, UK) was used to cut hippocampal slices (~400 µm). The slices were then maintained on Biopore™ membranes (Millicell standing inserts, Merck Millipore, Schwalbach, Germany). Exchange of culture medium (1 ml) was performed three times per week. The culture medium is composed of 50% minimal essential medium, 25% Hank's balanced salt solution (Sigma-Aldrich, Taufkirchen, Germany), 25% horse serum (Life Technologies, Darmstadt, Germany) and 2 mM L-glutamine (Life Technologies). Slices were kept in

a humidified atmosphere (5% CO_2, 36.5°C) in an incubator (Heracell, Thermo Scientific, Dreieich, Germany), and pH was maintained at 7.3. Slices with incomplete hippocampal formation were rejected.

Solutions and drugs

Slice cultures were constantly supplied with ACSF that contained: 129 mM NaCl, 3 mM KCl, 1.25 mM NaH_2PO_4, 1.8 mM $MgSO_4$, 1.6 mM $CaCl_2$, 21 mM $NaHCO_3$ and 10 mM glucose. A gas mixture of 95% O_2 and 5% CO_2 was used to saturate the recording solution and the pH was 7.4. For ACSF used in the submerged chamber, the concentration of $NaHCO_3$ was increased to 26 mM (see calcium imaging below). Salts, carbachol, and rotenone were all purchased from Sigma-Aldrich.

Gamma oscillations were induced by constant bath application of the muscarinic receptor agonist, carbachol (20 µM and 10 µM in the interface and the submerged chamber, respectively).

Electrophysiology

Experiments were conducted at 9–10 days in vitro (DIV) for recordings for spike sorting and at four to five weeks DIV for calcium imaging if not otherwise stated.

Intact Biopore™ membranes were inserted into the interface chamber supplied with pre-warmed ACSF at 34 ± 1°C. Cut Biopore™ membranes (with Vannas-Tübingen Spring scissor; 15008-08, Fine Science Tools GmbH, Heidelberg, Germany) were inserted in the submerged chamber for calcium imaging. Recording solution was pre-warmed at 32 ± 1°C. The flow of ACSF was 1.5–1.8 ml/min in the interface chamber and 8 ml/min in the submerged chamber. The fast flow in the submerged chamber ensures quick delivery of applied drugs (carbachol and rotenone) to all areas of the slice culture.[14] The ambient gas mixture in the interface chamber (95% O_2 and 5% CO_2) was supplied at a flow rate of 1.5 l/min.

Glass electrodes were made from GB150F-8P borosilicate filaments (Science Products GmbH, Hofheim, Germany) for LFP, and from GC120F-10 borosilicate filaments (Clark Electromedical Instruments, Reading, UK) for juxtacellular recording electrodes. Electrodes (tip diameter: 3–5 µm for LFP recordings and 1.5 µm for juxtacellular recordings) were pulled using Zeitz DMZ Puller (Zeitz-Instruments Vertriebs GmbH; Martinsried, Germany) and filled with recording solution. Mechanical micromanipulators (MX-4, Narishige International Ltd., London, UK) aided the positioning of electrodes in the targeted regions for recording. Recordings were performed using an EXT 10-2 F amplifier in EPMS-07 housing (npi electronic GmbH, Tamm, Germany). Recordings were low-pass filtered at 3 kHz and digitised at 10 kHz (LFP recordings) and 20 kHz (juxtacellular recordings) using CED 1401 interface and Spike2 software (Cambridge Electronic Design, Cambridge, UK) for storage of data on a computer disk for offline analysis.

We performed spike sorting based on recordings with metal electrodes made from tungsten wire (diameter: 12.5 µm; California Fine Wire Company, Grover Beach, CA, USA) in the interface chamber. Here, an EXT-T1M amplifier was used (npi electronic GmbH). Recordings were low-pass filtered at 3 kHz and digitised at 20 kHz using CED Power3 1401 interface (Cambridge Electronic Design).

Calcium imaging

Slice cultures were infected with adeno-associated virus (AAV) obtained from Penn Vector Core (Philadelphia, PA, USA) encoding GCaMP6f under the control of the CaMKII promoter (AAV5.CamKII.GCaMPf.WPRE.SV40, Lot # V5391MI-S). AAV transduction was achieved under sterile conditions by applying 0.8 µl of the viral particles solution (qTiter: 1.55e13 GC/ml) on top of the slices.

Imaging of the hippocampal CA3 region (with 20× magnification) was performed three to four weeks after viral infection, if not otherwise stated. Slices were maintained in the submerged chamber of Olympus BX51WI microscope (Olympus, Hamburg, Germany). GCaMP6f was excited at 485 ± 10 nm. Fluorescence images (emission at 521 ± 10 nm) were recorded at 4 Hz using a CCD camera (ORCA-ER; Hamamatsu Photonics, Hamamatsu City, Japan).

Before transferring slice cultures to the submerged chamber (10 µM carbachol) for imaging, persistent gamma oscillations were induced in the interface chamber (20 µM carbachol). Imaging was performed for 5 min during baseline gamma oscillations. Rotenone (0.1 µM) was then applied and after ~5 min imaging was resumed for additional 5 min during the mild metabolic stress condition.

Ensembles detection

Regions of interest (ROIs) representing the soma of pyramidal cells were drawn manually by the experimenter for each imaging session using Fiji.[45] The same ROIs enabled later identification of cells participating in synchronised activity and ensemble formation. A custom-made algorithm (Matlab 2018 b, MathWorks, Natick, MA, USA) was used to calculate the average fluorescence within ROIs after discarding cross-talk contamination (Supplementary Figure 3).

For determination of the background, a standard deviation projection was calculated, the darkest 5% was considered as background and subtracted from the average fluorescence. For visualisation of events (Figure 2(a) and (b)), F/F_o was calculated by relating the fluorescence values (F) to the baseline fluorescence (F_o).

For a true signal to be detected (Supplementary Figure 3(a)), two conditions have to be satisfied. First, traces from all pixels within the relevant ROI should show higher values (at least 95% of the pixels) than the baseline fit of the traces. This indicates that the whole ROI is fluorescing which occurs if a cell is active. However, out of focus background can increase pixel values in the ROI as well, leading to false positive signal. Therefore, the second condition is that the average pixel values from the surrounding region (border of the ROI) are lower than the values of pixels within the ROI (less than the lowest 5%).

On the contrary, when contamination of the complete ROI occurs (Supplementary Figure 3(b)), transients from the surrounding region are high enough relative to the values of pixels within the ROI (higher than the lowest 5%), thereby, violating the second condition described above. In this case, the difference between activity outside and within the ROI during the events was linearly interpolated between the beginning and end of the relevant event. In the case of partial overlap contamination (Supplementary Figure 3(c)), violation of the first condition occurs, in which only a portion of pixels show elevated transients. These pixels are clustered using K-means and their fluorescent transients are discarded from calculating the final average fluorescent signal.

For detection of synchronised activity, fluorescence transients were smoothed by sliding average window of 1 s. The pre-processed calcium traces were analysed as described before.[46] Fluorescence values (F) of each cell were normalised to their maximum F value across all frames. This yielded values between 0 and 1. As a next step, we identified time points, in which the ensemble activity was above chance. To this end, we first determined a threshold based on randomly shuffled data. F values for each cell were shifted randomly in time in a circular fashion (while maintaining individual cells activity), and the average network activity of each frame was measured. This step was repeated 10,000 times yielding a distribution of average network activities, which reflects randomised activity. From this distribution, we defined the 99th percentile as the threshold for 'above chance activity', which is referred to as synchronised activity in the text. Each frame with such synchronised activity is then described by an n-dimensional vector (population vector) containing the normalised F values, where n is the total number of cells. To identify recurring synchronised activity, we determined which of those frames showed similar patterns. To do this, we calculated a similarity matrix for all possible frame pairs. Similarity indices were calculated as the cosine of the angle between the two frame vectors. This yielded values between 0 and 1, where 1 corresponds to perfect similarity. The more similar the set of active cells in the compared events, the higher is the similarity index. Again a threshold for similarity was determined to identify stably recurring synchronised activity over random co-activity. As described above, the threshold was set to the 99th percentile of the similarity distribution of randomised population vectors (shifted randomly 10,000 times).

Afterwards, calcium transients were translated to binary output, in which recruited cells at the time points of synchronised activity were translated to logical ones (Figure 3(a)). The output is population vectors in binary code. These vectors were then categorised by principal component analysis,[47] followed by clustering using Fuzzy C-means and Dunn's index into ensembles of pyramidal cells (Figure 3(b)).[48]

Data analysis

Analysis of the electrophysiological signals was accomplished off-line using Spike2 and Matlab. To extract gamma oscillations for further analysis, LFP signals of 5 min were subdivided into segments of 30 s and band-pass filtered (fast Fourier transform, FFT, passband frequency: 5–200 Hz, 8th order).[15,49] For quantification of the gamma oscillations, the filtered traces were processed with Welch's algorithm and a fast Fourier transformation (FFT size: 8192) yielding the power spectral density plots used for calculation of characteristic features of gamma oscillations. Gamma oscillations were analysed for peak frequencies, peak power, full width at half-maximum (FWHM) and area under the curve (AuC) of power spectra using custom-made Matlab algorithms. FWHM reflects the synchrony of activated synapses. Spike sorting was performed using Wave_Clus.[42] First, signals were band-pass filtered (300–3000 Hz), then features of spikes were extracted using wavelet coefficients, followed by clustering of units. Parameters used for analysis are provided in Supplementary Table 1. We categorised sorted units according to their firing rates during baseline gamma oscillations. Based on our juxtacellular recordings and previous studies,[50,51] we set a threshold of 10 Hz for fast-spiking neural units (FSUs), and of 5 Hz for slow-spiking neural units (SSUs).

Data are collected from 'n' number of slices prepared from 'N' number of preparations, unless otherwise stated. Data are summarised by their median ± the interquartile range (IQR = 75% percentile – 25%

percentile), error bars indicate minimal and maximal values. Figures were generated using CorelDRAW X7 (Corel Corporation, Ottawa, Canada).

Statistical evaluation

Statistical analysis was performed using Prism 6 (GraphPad Software Inc., La Jolla, CA, USA). Shapiro–Wilk test was used to test for normality in the data distribution. Comparisons among paired data were made with paired *t*-test if normally distributed, otherwise Wilcoxon signed-rank test. Comparisons among unpaired data were made with unpaired *t*-test if normally distributed, otherwise Mann–Whitney test. To test for correlations, the correlation coefficient *r* and *p*-value were computed using the Pearson correlation. *p*-values less than 0.05 (indicated by asterisks) were considered to indicate a significant difference between compared groups. To test the difference between the cumulative distribution functions, we used two-sample Kolmogorov–Smirnov test. One-way ANOVA was applied with Holm-Sidak's multiple comparisons test for more than two groups.

Results

Mild metabolic stress attenuates gamma oscillations

We conducted LFP recordings in rat hippocampal slice cultures under submerged recording conditions. Bath-application of the cholinergic agonist carbachol reliably elicited gamma oscillations in the CA3 region (Figure 1 (a) and (b) and Supplementary Figure 1). Mild metabolic stress was induced by partial inhibition of mitochondrial ATP production. Compared to our previous study,[14] we used a lower concentration of rotenone.

Gamma oscillations were attenuated but not interrupted by rotenone. This was visible from the continuous decay, but there was clear persistence of gamma oscillations during rotenone application (Supplementary Figure 2). Quantitative analysis revealed a significant reduction in power and AuC derived from the power spectrograms by about 70% and 68%, respectively. In line with the persistence of the oscillation pattern, there were no significant changes in the frequency (*f*) or FWHM (Figure 1(c) to (f)). Since the reduction of power was less than one magnitude, we consider the induced level of metabolic stress as mild. We note that there was no pathological activity, such as spreading depolarization or epileptiform discharges, detected upon rotenone application (Figure 1(a) and (b)).

Our data show that a low concentration of rotenone causes mild metabolic stress, which attenuates gamma oscillations at the network level. To determine the effects at the cellular level, we performed calcium imaging simultaneously with LFP recordings during gamma oscillations at baseline and during rotenone-induced metabolic stress.

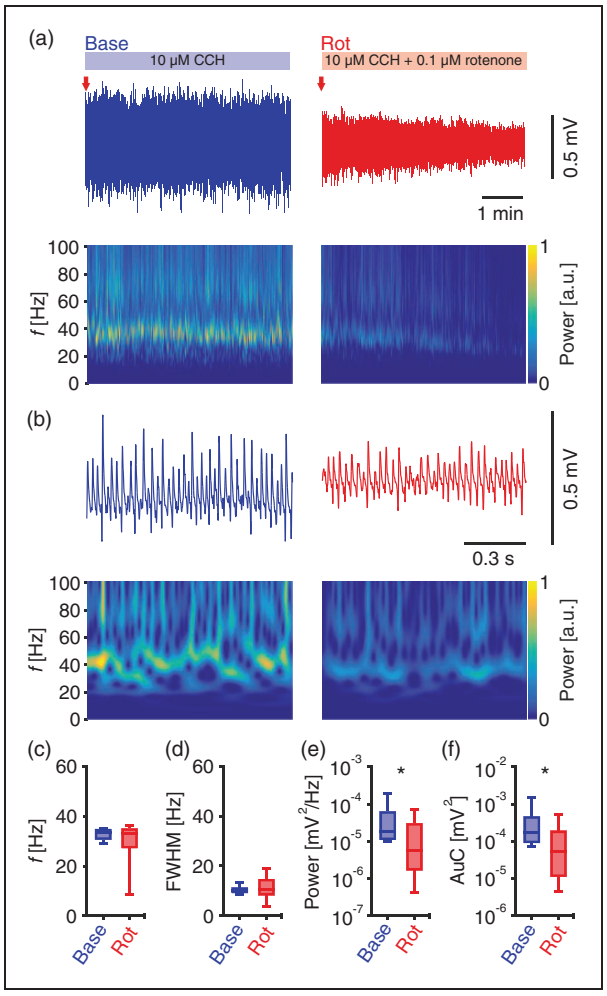

Figure 1. Gamma oscillations challenged by mild metabolic stress using rotenone. Local field potentials were recorded in submerged condition. (a) Sample traces of cholinergically induced gamma oscillations (blue, top left) and during additional application of rotenone (0.1 µM, red, top right). Red arrows indicate time points in (b) at higher temporal resolution. Corresponding wavelet transformations (bottom) showing the power of frequency domains over time. Heat-scale colours encode for power in arbitrary units (a.u.). Note that wavelet transformations during rotenone application are normalised to transformations during baseline. Gamma oscillations were analysed for different parameters for the shown duration of baseline (Base) and rotenone (Rot) application in (a). n/N slices/preparations: 8/3. (c) Peak frequency (*f*), Wilcoxon matched-pairs signed-rank test. (d) Full width at half-maximum (FWHM), paired *t*-test. (e) Peak of power spectral density (Power), Wilcoxon matched-pairs signed-rank test. (f) Area under the curve (AuC), Wilcoxon matched-pairs signed-rank test. $*p < 0.05$. Data are summarised by their median ± the interquartile range (IQR = 75% percentile − 25% percentile), error bars indicate minimal and maximal values.

Detection of synchronised activity during gamma oscillations

In order to identify ensembles, we used GCaMP6f driven by the CaMKII promoter to monitor the activity of multiple pyramidal cells. Calcium transients reflect action potentials as shown by juxtacellular recordings (Figure 2(a) and (b)). Large and small calcium transients reflect trains and single action potentials, respectively. The detected average firing rate of pyramidal cells (2.18 ± 0.96 Hz; mean $\pm$ SD, $n = 17$ cells from 17 slices from 5 preparations) is similar to previously reported ranges during gamma oscillations.[22,51]

To reduce cross-talk contamination resulting from overlapping somata occurring particularly in epifluorescence calcium imaging, we developed an algorithm that resamples the pixels used for re-constructing calcium transients (see Materials and methods and Supplementary Figure 3). The refined calcium transients were further analysed for detecting events of synchronised multicellular activity based on a previously described method.[46] These events indicate periods when pyramidal cells are co-active. The beginning of each event is marked with a black dot in Figure 2(c). The spatial distribution of a group of co-active cells (dashed rectangle in Figure 2(c)) is shown in Figure 2 (d). Although they are widely distributed (rather than overlapping), their activity appears to be highly synchronised (Figure 2(e), 'Base'). Note that the calcium imaging experiments reported in Figure 2(c) and (h) correspond to the LFP recordings in Figure 1.

Figure 2(f) shows the similarity between events of synchronised activity (black dots in Figure 2(c)). The similarity is based on comparing the set of contributing cells to these events. The brighter the heat-scale colour for any pair of compared events, the more similar is the set of pyramidal cells active during these events. These data show that repetitive patterns of synchronised activity (Figure 2(f)) can be reliably detected during gamma oscillations (Figure 2(e), left).

Mild metabolic stress disturbs synchrony but not the overall activity of pyramidal cells

Mild metabolic stress was sufficient to disturb the synchronised activity (Figure 2(e), right). We observed that the percentage of cells recruited into synchronised activity decreased by about 37% upon mild metabolic stress (Figure 2(g)). Moreover, the summed duration of all events spent in synchronised activity as a percentage of the recording period was significantly reduced by about 9% as well (Figure 2(h)). However, the overall activity of all pyramidal cells (quantified as AuC of calcium transients) showed no changes between both conditions (Figure 2(i)).

These findings demonstrate that recruiting groups of cells into synchronised patterns of activity is metabolically more sensitive than maintaining the overall activity.

Pyramidal cell ensembles are present during gamma oscillations

The above data revealed the effects of metabolic stress at the cellular level. We further aimed to investigate the effects at the level of neuronal ensembles. Thus, we grouped the contributing pyramidal cells from different events into ensembles. We first translated calcium transients into a binary output,[48] i.e. calcium transients of active cells during synchronised events are represented by logical 'ones'. The output of this operation is a set of population vectors (red arrows in Figure 3(a)), which were then categorised into ensembles (Figure 3(b) to (d)) by principal component analysis,[47] followed by clustering.[48]

We observed that most of the detected cells are recruited into ensembles. We also investigated whether there is a difference in the number of cells participating only in a single or multiple ensembles. The lack of any significant difference (Figure 3(e)) indicates that a fixed portion ($\sim$50%) of the detected cells is recruited in ensemble formation. The number of detected ensembles ranged from one to three per slice (Figure 3(f)). A total of 17 ensembles from all slices showed an average of 58.5 ± 34.2 constituent cells (mean $\pm$ SD, $n = 8$ slices from 3 preparations). To determine whether slices with a low number of active cells hindered ensembles detection, we calculated correlations between the number of cells, events and detected ensembles (Figure 3(f) to (h)). The absence of any correlation suggests that the number of detected cells and events reflects the intrinsic activity underlying gamma oscillations and did not hinder the detection of ensembles.

These findings reveal the existence of pyramidal cell ensembles, which are reproducibly activated during gamma oscillations.

Ensembles are disturbed and pyramidal cells are partially disinhibited during mild metabolic stress

We examined how individual pyramidal cells (recruited in ensembles) behave upon mild metabolic stress compared to their activity during baseline gamma oscillations. In the example shown in Figure 3, we observed an increase in the activity of pyramidal cells (Figure 3 (i)). We next normalised the activity of individual cells (during baseline and metabolic stress) to the average activity of their corresponding ensemble during baseline. This was performed for all cells from all slices. For better visualisation, the normalised activity of cells was

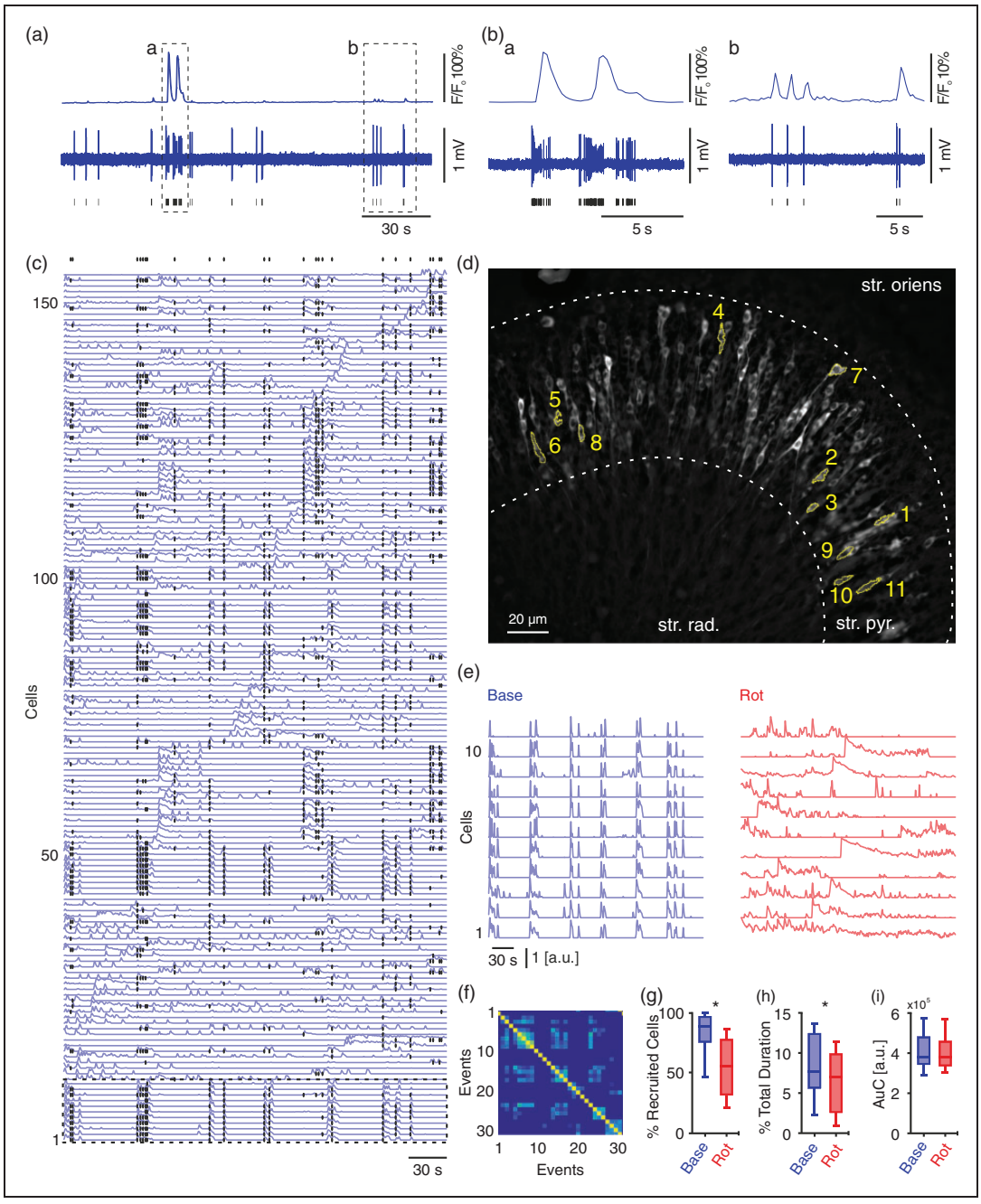

Figure 2. Mild metabolic stress attenuates synchronised but not overall activity of pyramidal cells during gamma oscillations. Calcium fluorescence and simultaneous juxtacellular signals were recorded in submerged condition. (a) Traces of calcium fluorescence (top) with corresponding cell activity (juxtacellular recording, middle). Black lines indicate times of action potentials fired by recorded cell (bottom). Dashed rectangles (a–b) indicate traces at higher resolution in (Ba-b). (c) Traces of calcium fluorescence for all detected cells ($n = 155$) in one slice. Black dots (top) indicate beginnings of periods of synchronised activity and participating cells. Dashed rectangle (bottom) marks the 11 cells represented in (d–e). (d) Standard deviation projection of calcium fluorescence for the whole acquisition time during baseline gamma oscillations (5 min). Note that the highlighted cells elicit synchronised activity (in (e), left). str. oriens, Stratum oriens; str. pyr., Stratum pyramidale; str. rad., Stratum radiatum. (e) Highlighted cells in (c–d) show synchronised activity during baseline gamma oscillations (blue, left) while in the presence of rotenone activity shifts to a less synchronised pattern (red, right). (f) Similarity matrix for events of synchronised activity (marked with black dots in (c)). Note the bright blue spots far from the diagonal. The brighter, the more similar the set of active cells in compared events. This indicates that these set of cells are repetitively active. Synchronised and overall activity were analysed for different parameters. For cells/slices/preparations: 713/8/3. (g) Percentage of recruited cells during synchronised activity. (h) Percentage of the summed duration of the synchronised activity. (i) Area under the curve (AuC) for calcium fluorescence, reflecting the overall activity of pyramidal cells. (g–i) paired *t*-test, $^*p < 0.05$. Data are summarised by their median ± the interquartile range (IQR = 75% percentile – 25% percentile), error bars indicate minimal and maximal values.

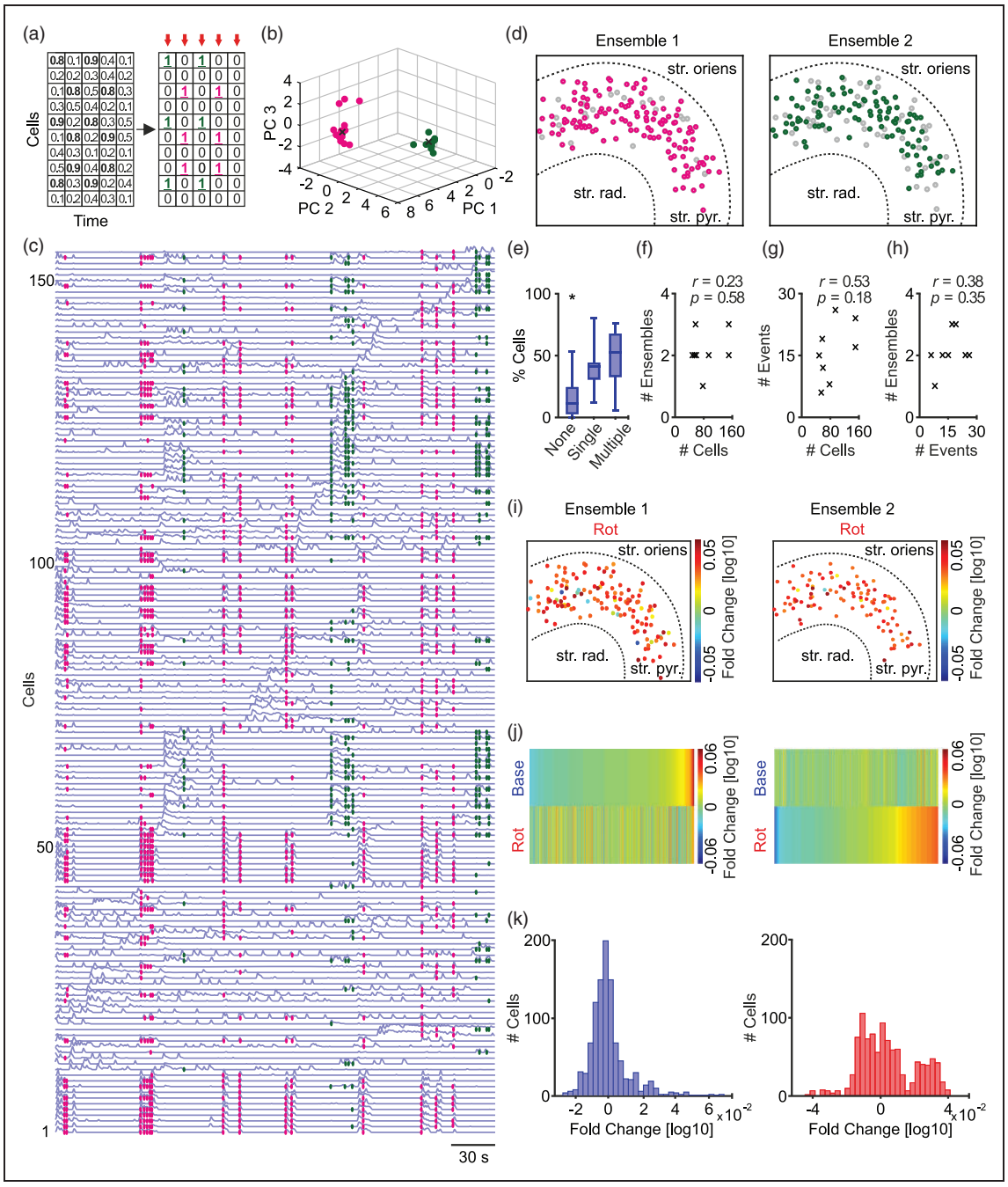

Figure 3. Clustering events of synchronised activity to identify neuronal ensembles. (a) Transferring calcium fluorescence transients into binary population vectors (red arrows). (b) Principal component analysis applied to categorise vectors in the first three principal components, followed by Fuzzy C-means clustering with the aid of Dunn's index (black crosses; the centre of clusters). (c) Traces of calcium fluorescence for all detected cells in one slice with colour-coded events according to the ensembles clustered in (b). (d) Spatial map of cells belonging to the two identified ensembles corresponding to the shown example. Data were analysed for different parameters. n/N slices/preparations: 8/3. Grey circles represent cells not recruited into the presented ensemble. str. oriens, Stratum oriens; str. pyr., Stratum pyramidale; str. rad., Stratum radiatum. (e) Difference between cells recruited in only one ensemble or multiple ensembles or none. One-way ANOVA with Holm-Sidak's multiple comparisons test, $^*p < 0.05$. (f–h) Correlations between numbers of identified cells, events and ensembles. No significant correlation is observed. (i) Spatial map (similar to (d)) showing fold change in AuC of cells' activity during mild metabolic stress in relation to their individual activity during baseline gamma oscillations. (j) Activity of each cell is normalised to the average activity of their corresponding ensemble, followed by sorting according to baseline gamma oscillation (top left) or mild metabolic stress (bottom right). (k) Histogram of cells' sorted activity (analogous to top left and bottom right in (j)). Note the multimodal distribution (right), and the shift of pyramidal cells to be more active upon mild stress, two-sample Kolmogorov–Smirnov test ($D = 0.226$, $p < 0.05$). Data are summarised by their median ± the interquartile range (IQR = 75% percentile – 25% percentile), error bars indicate minimal and maximal values.

sorted for both conditions (Figure 3(j)). The corresponding distributions are shown in Figure 3(k). During metabolic stress, a shift towards increased activity is observed (Figure 3(k), right).

Although the overall activity of all cells showed no significant difference (Figure 2(i)), we observed an increase of pyramidal cell activity at the ensemble level during mild metabolic stress. Our findings show that the formation of ensembles is disturbed, probably by partial disinhibition of pyramidal cells.

Mild metabolic stress primarily leads to disinhibition of slow-spiking units

To further elucidate the underlying mechanism, we studied the changes in the firing patterns of slow- and fast-spiking neural units (SSUs, FSUs) in response to metabolic stress. Recordings were done in an interface chamber under conditions comparable to the induced mild metabolic stress under submerged conditions (Figure 1). Similar to our previous data, the power of gamma oscillations and the AuC were significantly reduced by about 51% and 43%, respectively, whereas frequency and FWHM were unchanged (Figure 4). Neuronal spikes were recorded with tungsten-electrodes and then sorted with an algorithm based on wavelet transformations of high-pass filtered spikes (Figure 5(a)).[42]

We were able to distinguish between different units and determined their firing rates (Figure 5(b) and (c)). Based on this data, we categorised neural units into FSUs (>10 Hz) and SSUs (<5 Hz). While FSUs maintained their firing rate (Figure 5(d)), SSUs increased their firing rate by about 137% during mild metabolic stress (Figure 5(e)). These findings further support our previous observation that pyramidal cells, which are likely represented by the SSUs, are partially disinhibited upon mild metabolic stress.

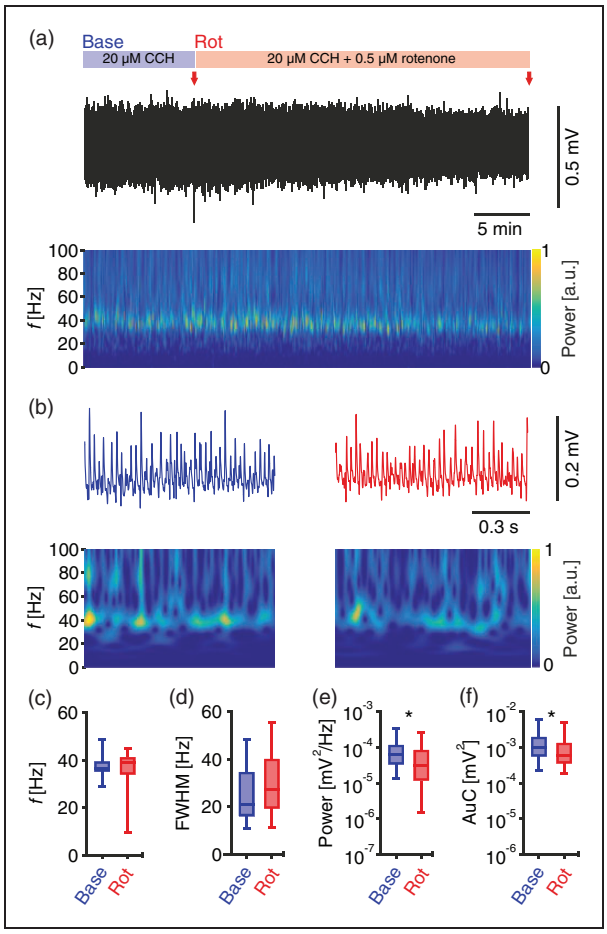

Figure 4. Mild metabolic stress of gamma oscillations in interface condition. (a) Sample trace of LFP recording in interface chamber during baseline gamma oscillations (first 10 min) and additional application of 0.5 µM rotenone. Red arrows indicate time points in (b) at higher temporal resolution. Corresponding wavelet transformation (bottom) showing the power of frequency domains over time. Heat-scale colours encode for power in arbitrary units (a.u.). Note that wavelet transformations during rotenone application are normalised to transformations during baseline. Gamma oscillations were analysed for different parameters for the last 5 min in each phase (baseline and rotenone application), n/N slices/preparations: 34/6. (c) Peak frequency (*f*). (d) Full width at half-maximum (FWHM). (e) Peak of power spectral density (Power). (f) Area under the curve (AuC). (c–f) Wilcoxon matched-pairs signed-rank test. $*p < 0.05$. Data are summarised by their median ± the interquartile range (IQR = 75% percentile – 25% percentile), error bars indicate minimal and maximal values.

Discussion

Organotypic hippocampal slice cultures as a model for studying neuronal ensembles

Gamma oscillations can be induced in situ by different pharmacological, electrical and optogenetic approaches.[17,52] We employed the cholinergic model of gamma oscillations, which mimics cholinergic input from the septum to the hippocampus during exploratory behaviour in vivo.[22,34,53]

Gamma oscillations in slice cultures are known to show properties that are comparable to gamma oscillations in acute slice preparations. (1) Oscillations are mostly at ~40 Hz and are generated in the CA3 region.[30,53] (2) The phase of gamma oscillations shows a reversal in polarity of LFP recordings between signals recorded from *stratum pyramidale* and *stratum radiatum*.[22,54] (3) Pyramidal cells fire at low rates in slice cultures (Figure 2(a) and (b)) and in acute slices during gamma oscillations.[51] Additionally, comparable developmental properties to the hippocampus in vivo are observed. This includes the maturation of interneurons and the expression of parvalbumin.[55,56] However, the inclusion of ventral and dorsal

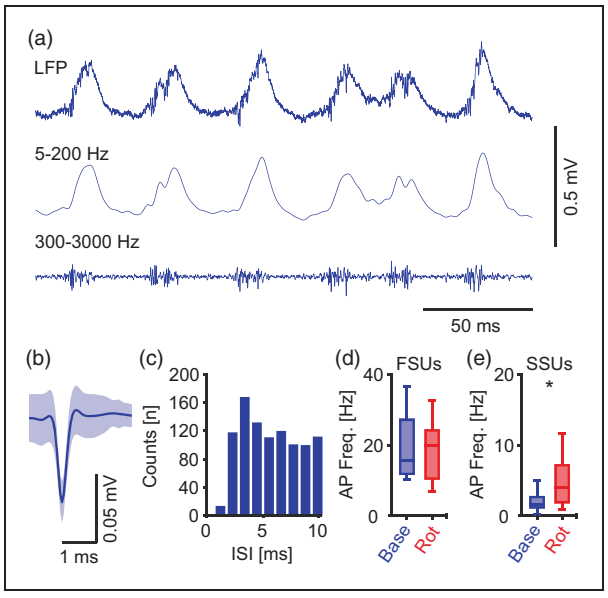

Figure 5. Slow-spiking units are selectively disinhibited during mild metabolic stress. (a) Sample trace of original LFP recording (top), band-pass filtered at 5–200 Hz and 300–3000 Hz (middle and bottom respectively), highlighting gamma oscillations and units firing. (b) Sample of a fast-spiking unit, mean ± SD. (c) Inter-spike interval (ISI) for the unit in (b) during baseline gamma oscillations. (d–e) Units/slices/preparations: 18/18/6. (d) Action potential (AP) frequency for units with >10 AP/s during baseline, Wilcoxon matched-pairs signed-rank test. (e) AP frequency for units with <5 AP/s during baseline, paired *t*-test. FSUs and SSUs; fast- and slow- spiking units respectively. *$p < 0.05$. Data are summarised by their median ± the interquartile range (IQR = 75% percentile – 25% percentile), error bars indicate minimal and maximal values.

hippocampal tissue, the long-term maintenance of slice cultures as well as the induction of only mild metabolic stress in the experiments likely contributed the large variability in some of our readouts. Further in situ and in vivo studies are required to substantiate the functional relevance of our data.

For our study, slice cultures are superior to acute slices, since damaged surface layers are removed during the culture period,[57] thereby offering clearer morphology for live-cell imaging. Their capability of expressing gamma oscillations after more than four weeks,[30] provided a sufficient period for the expression of GCaMP6f.[37,40] It should be taken into account that in vitro and in situ models generally differ from in vivo conditions. However, slice cultures used in this study are maintained on Biopore™ membranes in the incubator under near physiological conditions, in which the glucose concentration is about 4 mM,[30] and the partial oxygen pressure in the core of the slice is about 60 mmHg.[58] Additionally, the presence of ramified microglia (tissue-resident brain macrophages), the minimal release of pro-inflammatory cytokines as well as the absence of a glial scar indicate excellent tissue preservation.[49] However, increased glucose and oxygen supply during the recordings is necessary for maintaining energy-demanding gamma oscillations, especially in submerged conditions.[12,14]

Detection of pyramidal cell ensembles during gamma oscillations

The stability of gamma oscillations in the submerged condition for at least 25 min (Supplementary Figure 1) provided a sufficient period for robust analysis of baseline recording and the induction of metabolic stress (Supplementary Figure 1). Despite the low temporal resolution of calcium imaging, the high spatial resolution enabled the monitoring of a large pyramidal cell population at the same time thus permitting the detection of pyramidal cell ensembles.[21,38,39,46]

We developed an algorithm (Supplementary Figure 3) for reducing cross-talk contamination among different regions of interest (ROIs). Pixels reporting contaminated signals are detected and further discarded from constructing calcium fluorescence transients. We applied previously described methods[46] for detection of synchronised activity that reflects periods when pyramidal cells are co-active (Figure 2(c)). Subsequently, co-active pyramidal cells were grouped into ensembles.[48] In this study, we define an ensemble as a group of co-active neurons with a repetitive pattern of activity.

The detected ensembles showed repetitive patterns of active cells during gamma oscillations. A closer analysis revealed that the difference in the number of detected cells in different slices did not affect the final number of identified ensembles (Figure 3(f) to (h)). Besides, we found no difference between the numbers of cells recruited in one or multiple ensembles, indicating that at any time point a fixed portion of pyramidal cells is recruited in ensembles formation (Figure 3(e)).

Ensembles are disturbed and pyramidal cells are partially disinhibited upon mild stress

In this study, we applied mild metabolic stress using low concentrations of rotenone (0.1 µM and 0.5 µM in submerged and interface recording chambers, respectively). Rotenone is a highly selective complex I inhibitor, and its lipophilic nature enables penetration of cells and rapid interference with mitochondrial function and production of ATP.[35,44,59] The resulting reduction of neuronal activity can be observed within a few minutes.[14,43] We consider the metabolic stress to be mild since the observed reduction of power is only about one magnitude and the gamma-band frequency oscillations are still preserved (Figures 1 and 4).

A stronger stress level[13,14] would have hindered to reveal the most vulnerable neuronal population by suppressing the whole network.

We quantified the changes in the synchrony of the network during baseline gamma oscillations and upon metabolic stress. In all slices, we observed a significant reduction in the number of cells that participated in synchronised activity (Figure 2(g)). In addition, the total time spent in synchronised activity was significantly reduced (Figure 2(h)). Although there was only little reduction (by about 9%), the effect was present in seven out of eight slices. Taking into account, that the time pyramidal cells spent in synchronised activity was rather low already during baseline gamma oscillations, a further reduction by 9% was sufficient to disturb ensemble formation. Both measures reflect the disorganised activity of pyramidal cells during mild metabolic stress.

We further quantified the overall activity of pyramidal cells by measuring the AuC of calcium transients for all cells (Figure 2(i)). Interestingly, we found no significant changes during metabolic stress. This widely excludes that the reduction in the synchronised activity is caused by a reduction in the activity of the cells. On the contrary, it indicates that mild metabolic stress is not sufficient to reduce the activity of pyramidal cells. Additionally, these findings might indicate that eliciting synchronised activity is metabolically more sensitive than maintaining the overall activity.

Following the grouping of cells into ensembles, we normalised the activity of individual cells (during baseline and metabolic stress) to the average activity of their corresponding ensemble during baseline. We observed that some pyramidal cells show an increase in their activity during mild metabolic stress, which is reflected by the shift towards higher excitability (Figure 3(k)). These findings indicate that pyramidal cells, which are recruited into ensembles, are partially disinhibited during mild metabolic stress.

Pyramidal cells are believed to compute, store and retrieve information during higher brain functions.[22,60] Precise spatial and temporal matrices are necessary for these cells to elicit synchronised activity patterns. It is known that inhibitory interneurons, especially fast-spiking interneurons, play a key role in controlling and synchronising the activity of pyramidal cells during gamma oscillations.[22,61–63] Several of their features indicate a high energy demand.[19] These include (1) their fast-spiking behaviour;[64] (2) equipment with mitochondria of large size and number;[65] (3) enrichment of the mitochondria with complex IV and cytochrome *c*, which are necessary for the electron transport chain;[66] (4) innervation of large number (~2000) of pyramidal cells with their massive axonal arborisation.[67]

Our study shows that (1) synchronised activity of pyramidal cells is more vulnerable than the overall activity and (2), at the ensemble level, pyramidal cells are partially disinhibited during mild metabolic stress. Considering the presumed high energy demand of fast-spiking interneurons,[19] and our new findings, we conclude that the observed effects likely result from alterations in the function of fast-spiking interneurons. Therefore, mild metabolic stress might disturb interneuron function prior to pyramidal cell function. Our conclusion supports the concept that interneurons are exquisitely vulnerable to metabolic stress during fast brain oscillations.[19]

A mechanism for the alteration of gamma oscillations

Fast-spiking interneurons generate action potentials during gamma oscillations almost phase-locked to each cycle.[62,68] Therefore, the fast release of GABA leads to rhythmic inhibition in a large population of pyramidal cells. Synchronised inhibitory postsynaptic potentials in *stratum pyramidale* rather than excitatory postsynaptic potentials or action potentials shape gamma oscillations in LFP recordings.[63,69–73] Therefore, the reduction in power of gamma oscillations during metabolic stress might result from a failure in maintaining firing rates and/or a disturbance in the presynaptic terminal. The differences in the reduction of power in slices recorded in the interface chamber (Figure 4(e)) and in slices recorded in the submerged chamber (Figure 5(e)) probably resulted from differences in flow speed and exchange dynamics of the recording solution.

It was predicted that the energy demand for action potential generation and postsynaptic ion fluxes is higher than for processes at the presynaptic terminal.[74–77] On the other hand, it was shown that energy demands for presynaptic processes like Ca^{2+} removal, transmitter release, and uptake as well as vesicles turnover require more energy than previously expected.[78]

In fast-spiking interneurons, such as parvalbumin-positive GABAergic basket cells, the presynaptic terminal is well equipped to maintain fast and precise transmitter release. The terminals contain mainly P/Q-type Ca^{2+} channels,[79–82] which are known for their fast gating in comparison to other Ca^{2+} channels.[83] Additionally, Ca^{2+} channels are tightly coupled to release sensors at the presynaptic terminal.[79,84,85] Furthermore, fast and precise firing is energetically demanding and the presynaptic terminals appear to have adapted for such function. Their terminals are enriched with more and larger mitochondria.[65] The mitochondrial ultrastructure has adapted as well for

the fast-spiking function, as indicated by their high amounts of cytochrome *c*.[65,66] Additionally, mitochondria in highly active synapses were found to have higher crista membrane density and lamellarity.[86] Overall, this indicates that slight disturbances in energy supply (e.g. during mild metabolic stress) are sufficient to disturb the function of fast-spiking interneurons, likely starting with alterations in the presynaptic terminal, which needs to be explored in detail in future studies.

We show that the activity of neural SSUs is increased during mild metabolic stress (Figure 5(e)). SSUs appear to be disinhibited, most likely because of lacking inhibition from interneurons being highly vulnerable to metabolic stress. Interestingly, firing rates of FSUs were not affected although the power of gamma oscillations was significantly reduced. Therefore, these findings might indicate that the loss of gamma oscillations begins with failures occurring at the presynaptic terminal of fast-spiking interneurons before changes in firing rates appear. Previous studies also showed that presynaptic function can be severely disrupted upon minimal interference with ATP synthesis.[76,87]

Conclusion

Gamma oscillations represent a functional brain rhythm involved in higher cognitive functions.[8,17,18,88] Inducing mild metabolic stress in slice preparations aims to mimic alterations in oxygen and energy substrate supply that also associate with the decline (rather than loss) in cognitive functions in vivo. These disturbances occur in cardiovascular diseases and, perhaps, aging and Alzheimer's disease.[23–25,89] They occur as well in mitochondrial diseases associated with impaired mitochondrial function and oxidative stress.[26–28]

In summary, the vulnerability of synchronised activity, the disturbance of pyramidal cell ensembles and the observed disinhibition of neural SSUs indicate the involvement of fast-spiking units. We interpret these findings as an indirect evidence for the high vulnerability of certain inhibitory cells. Additionally, we consider the presynaptic terminal as the 'Achilles heel' during mild metabolic stress, which supports the 'interneuron energy hypothesis'.[19] Furthermore, the findings provide a putative link between disturbances at the cellular level and cognitive dysfunction upon metabolic brain insults such as ischemia.[90] Further studies at the subcellular level might provide deeper insights into the mechanisms that underlie the breakdown of ensemble formation during metabolic stress evident from our multicellular investigation.

Funding

The author(s) disclosed receipt of the following financial support for the research, authorship, and/or publication of this article: This study was supported by SFB1134 (B02 and A03) from the German Research Foundation (DFG).

Acknowledgements

The authors would like to acknowledge Hilmar Bading, Bruno Chausse and Martin Kaiser for their help and support to this project. Special thanks to Andreas Draguhn for the helpful discussion.

Authors' contributions

SE, JOH, and OK conceptualised and designed the research. SE, AL, and JS performed research. SE, MB, JCB, DH, and JOH analysed data. SE, JOH, and OK interpreted the data. SE, JOH, and OK wrote the manuscript. All authors have revised and approved the final version of the manuscript and agree to be accountable for all aspects of the work.

Declaration of conflicting interests

The author(s) declared no potential conflicts of interest with respect to the research, authorship, and/or publication of this article.

ORCID iDs

Jan-Oliver Hollnagel https://orcid.org/0000-0002-4060-0022
Oliver Kann https://orcid.org/0000-0003-4365-8067

Supplemental material

Supplemental material for this article is available online.

References

1. Erecińska M and Silver IA. Tissue oxygen tension and brain sensitivity to hypoxia. *Respir Physiol* 2001; 128: 263–276.
2. Rolfe DF and Brown GC. Cellular energy utilization and molecular origin of standard metabolic rate in mammals. *Physiol Rev* 1997; 77: 731–758.
3. Williams LR and Leggett RW. Reference values for resting blood flow to organs of man. *Clin Phys Physiol Meas* 1989; 10: 187–217.
4. Hansen AJ. Effect of anoxia on ion distribution in the brain. *Physiol Rev* 1985; 65: 101–148.
5. Kann O. The energy demand of fast neuronal network oscillations: insights from brain slice preparations. *Front Pharmacol* 2012; 2: 90.
6. Shulman RG, Hyder F and Rothman DL. Lactate efflux and the neuroenergetic basis of brain function. *NMR Biomed* 2001; 14: 389–396.
7. Verweij BH, Amelink GJ and Muizelaar JP. Current concepts of cerebral oxygen transport and energy metabolism after severe traumatic brain injury. *Prog Brain Res* 2007; 161: 111–124.

8. Kann O, Papageorgiou IE and Draguhn A. Highly energized inhibitory interneurons are a central element for information processing in cortical networks. *J Cereb Blood Flow Metab* 2014; 34: 1270–1282.
9. Buzsáki G and Draguhn A. Neuronal oscillations in cortical networks. *Science* 2004; 304: 1926–1929.
10. Colgin LL. Rhythms of the hippocampal network. *Nat Rev Neurosci* 2016; 17: 239–249.
11. Uhlhaas PJ and Singer W. Abnormal neural oscillations and synchrony in schizophrenia. *Nat Rev Neurosci* 2010; 11: 100–113.
12. Galow LV, Schneider J, Lewen A, et al. Energy substrates that fuel fast neuronal network oscillations. *Front Neurosci* 2014; 8: 398.
13. Huchzermeyer C, Albus K, Gabriel HJ, et al. Gamma oscillations and spontaneous network activity in the hippocampus are highly sensitive to decreases in pO_2 and concomitant changes in mitochondrial redox state. *J Neurosci* 2008; 28: 1153–1162.
14. Kann O, Huchzermeyer C, Kovács R, et al. Gamma oscillations in the hippocampus require high complex I gene expression and strong functional performance of mitochondria. *Brain* 2011; 134: 345–358.
15. Schneider J, Berndt N, Papageorgiou IE, et al. Local oxygen homeostasis during various neuronal network activity states in the mouse hippocampus. *J Cereb Blood Flow Metab* 2019; 39: 859–873.
16. Buzsáki G and Wang XJ. Mechanisms of gamma oscillations. *Annu Rev Neurosci* 2012; 35: 203–225.
17. Bartos M, Vida I and Jonas P. Synaptic mechanisms of synchronized gamma oscillations in inhibitory interneuron networks. *Nat Rev Neurosci* 2007; 8: 45–56.
18. van Vugt MK, Schulze-Bonhage A, Litt B, et al. Hippocampal gamma oscillations increase with memory load. *J Neurosci* 2010; 30: 2694–2699.
19. Kann O. The interneuron energy hypothesis: implications for brain disease. *Neurobiol Dis* 2016; 90: 75–85.
20. Yuste R. From the neuron doctrine to neural networks. *Nat Rev Neurosci* 2015; 16: 487–497.
21. Carrillo-Reid L, Yang W, Kang Miller JE, et al. Imaging and optically manipulating neuronal ensembles. *Annu Rev Biophys* 2017; 46: 271–293.
22. Hájos N and Paulsen O. Network mechanisms of gamma oscillations in the CA3 region of the hippocampus. *Neural Netw* 2009; 22: 1113–1119.
23. Love S and Miners JS. Cerebrovascular disease in ageing and Alzheimer's disease. *Acta Neuropathol* 2016; 131: 645–658.
24. Pluta R, Jabłoński M, Ułamek-Kozioł M, et al. Sporadic Alzheimer's disease begins as episodes of brain ischemia and ischemically dysregulated Alzheimer's disease genes. *Mol Neurobiol* 2013; 48: 500–515.
25. Riddle DR, Sonntag WE and Lichtenwalner RJ. Microvascular plasticity in aging. *Ageing Res Rev* 2003; 2: 149–168.
26. Burté F, Carelli V, Chinnery PF, et al. Disturbed mitochondrial dynamics and neurodegenerative disorders. *Nat Rev Neurol* 2014; 11: 11–24.
27. Morán M, Moreno-Lastres D, Marín-Buera L, et al. Mitochondrial respiratory chain dysfunction: implications in neurodegeneration. *Free Radic Biol Med* 2012; 53: 595–609.
28. Zsurka G and Kunz WS. Mitochondrial involvement in neurodegenerative diseases. *IUBMB Life* 2013; 65: 263–272.
29. Gähwiler BH, Capogna M, Debanne D, et al. Organotypic slice cultures: a technique has come of age. *Trends Neurosci* 1997; 20: 471–477.
30. Schneider J, Lewen A, Ta TT, et al. A reliable model for gamma oscillations in hippocampal tissue. *J Neurosci Res* 2015; 93:1067–1078.
31. Freund TF and Katona I. Perisomatic inhibition. *Neuron* 2007; 56: 33–42.
32. Müller W and Misgeld U. Slow cholinergic excitation of guinea pig hippocampal neurons is mediated by two muscarinic receptor subtypes. *Neurosci Lett* 1986; 67: 107–112.
33. Nabekura J, Ebihara S and Akaike N. Muscarinic receptor activation of potassium channels in rat dentate gyrus neurons. *J Neurophysiol* 1993; 70: 1544–1552.
34. Marrosu F, Portas C, Mascia MS, et al. Microdialysis measurement of cortical and hippocampal acetylcholine release during sleep-wake cycle in freely moving cats. *Brain Res* 1995; 671: 329–332.
35. Sherer TB, Betarbet R, Testa CM, et al. Mechanism of toxicity in rotenone models of Parkinson's disease. *J Neurosci* 2003; 23: 10756–10764.
36. Einevoll GT, Kayser C, Logothetis NK, et al. Modelling and analysis of local field potentials for studying the function of cortical circuits. *Nat Rev Neurosci* 2013; 14: 770–785.
37. Chen TW, Wardill TJ, Sun Y, et al. Ultrasensitive fluorescent proteins for imaging neuronal activity. *Nature* 2013; 499: 295–300.
38. Grienberger C and Konnerth A. Imaging calcium in neurons. *Neuron* 2012; 73: 862–885.
39. Kwan AC. What can population calcium imaging tell us about neural circuits? *J Neurophysiol* 2008; 100: 2977–2980.
40. Podor B, Hu YL, Ohkura M, et al. Comparison of genetically encoded calcium indicators for monitoring action potentials in mammalian brain by two-photon excitation fluorescence microscopy. *Neurophotonics* 2015; 2: 021014.
41. Buzsáki G. Large-scale recording of neuronal ensembles. *Nat Neurosci* 2004; 7: 446–451.
42. Quiroga RQ, Nadasdy Z and Ben-Shaul Y. Unsupervised spike detection and sorting with wavelets and superparamagnetic clustering. *Neural Comput* 2004; 16: 1661–1687.
43. Kann O, Kovács R and Heinemann U. Metabotropic receptor-mediated Ca^{2+} signaling elevates mitochondrial Ca^{2+} and stimulates oxidative metabolism in hippocampal slice cultures. *J Neurophysiol* 2003; 90: 613–621.
44. Kann O, Schuchmann S, Buchheim K, et al. Coupling of neuronal activity and mitochondrial metabolism as revealed by NAD(P)H fluorescence signals in organotypic hippocampal slice cultures of the rat. *Neuroscience* 2003; 119: 87–100.
45. Schindelin J, Arganda-Carreras I, Frise E, et al. Fiji: an open-source platform for biological-image analysis. *Nat Methods* 2012; 9: 676–682.

46. Hamm JP, Peterka DS, Gogos JA, et al. Altered cortical ensembles in mouse models of schizophrenia. *Neuron* 2017; 94: 153–167.e8.
47. Pfeiffer T, Draguhn A, Reichinnek S, et al. Optimized temporally deconvolved Ca^{2+} imaging allows identification of spatiotemporal activity patterns of CA1 hippocampal ensembles. *Neuroimage* 2014; 94: 239–249.
48. Sasaki T, Matsuki N and Ikegaya Y. Metastability of active CA3 networks. *J Neurosci* 2007; 27: 517–528.
49. Ta TT, Dikmen HO, Schilling S, et al. Priming of microglia with IFN-γ slows neuronal gamma oscillations in situ. *Proc Natl Acad Sci U S A* 2019; 116: 4637–4642.
50. Csicsvari J, Hirase H, Czurkó A, et al. Oscillatory coupling of hippocampal pyramidal cells and interneurons in the behaving rat. *J Neurosci* 1999; 19: 274–287.
51. Zemankovics R, Veres JM, Oren I, et al. Feedforward inhibition underlies the propagation of cholinergically induced gamma oscillations from hippocampal CA3 to CA1. *J Neurosci* 2013; 33: 12337–12351.
52. Kann O, Hollnagel JO, Elzoheiry S, et al. Energy and potassium ion homeostasis during gamma oscillations. *Front Mol Neurosci* 2016; 9: 47.
53. Fisahn A, Pike FG, Buhl EH, et al. Cholinergic induction of network oscillations at 40 Hz in the hippocampus *in vitro*. *Nature* 1998; 394: 186–189.
54. Vodovozov W, Schneider J, Elzoheiry S, et al. Metabolic modulation of neuronal gamma-band oscillations. *Pflugers Arch* 2018; 470: 1377–1389.
55. Hasam-Henderson LA, Gotti GC, Mishto M, et al. NMDA-receptor inhibition and oxidative stress during hippocampal maturation differentially alter parvalbumin expression and gamma-band activity. *Sci Rep* 2018; 8: 9545.
56. Tsintsadze V, Minlebaev M, Suchkov D, et al. Ontogeny of kainate-induced gamma oscillations in the rat CA3 hippocampus *in vitro*. *Front Cell Neurosci* 2015; 9: 195.
57. Bahr BA, Kessler M, Rivera S, et al. Stable maintenance of glutamate receptors and other synaptic components in long-term hippocampal slices. *Hippocampus* 1995; 5: 425–439.
58. Huchzermeyer C, Berndt N, Holzhütter HG, et al. Oxygen consumption rates during three different neuronal activity states in the hippocampal CA3 network. *J Cereb Blood Flow Metab* 2013; 33: 263–271.
59. Schuchmann S, Kovacs R, Kann O, et al. Monitoring NAD(P)H autofluorescence to assess mitochondrial metabolic functions in rat hippocampal-entorhinal cortex slices. *Brain Res Brain Res Protoc* 2001; 7: 267–276.
60. Lisman J and Buzsáki G. A neural coding scheme formed by the combined function of gamma and theta oscillations. *Schizophr Bull* 2008; 34: 974–980.
61. Agetsuma M, Hamm JP, Tao K, et al. Parvalbumin-positive interneurons regulate neuronal ensembles in visual cortex. *Cereb Cortex* 2018; 28: 1831–1845.
62. Gulyás AI, Szabó GG, Ulbert I, et al. Parvalbumin-containing fast-spiking basket cells generate the field potential oscillations induced by cholinergic receptor activation in the hippocampus. *J Neurosci* 2010; 30: 15134–15145.
63. Penttonen M, Kamondi A, Acsády L, et al. Gamma frequency oscillation in the hippocampus of the rat: intracellular analysis *in vivo*. *Eur J Neurosci* 1998; 10: 718–728.
64. Hu H, Gan J and Jonas P. Interneurons. Fast-spiking, parvalbumin^{+} GABAergic interneurons: from cellular design to microcircuit function. *Science* 2014; 345: 1255263.
65. Takács VT, Szőnyi A, Freund TF, et al. Quantitative ultrastructural analysis of basket and axo-axonic cell terminals in the mouse hippocampus. *Brain Struct Funct* 2015; 220: 919–940.
66. Gulyás AI, Buzsáki G, Freund TF, et al. Populations of hippocampal inhibitory neurons express different levels of cytochrome *c*. *Eur J Neurosci* 2006; 23: 2581–2594.
67. Freund TF. Interneuron diversity series: rhythm and mood in perisomatic inhibition. *Trends Neurosci* 2003; 26: 489–495.
68. Hájos N, Pálhalmi J, Mann EO, et al. Spike timing of distinct types of GABAergic interneuron during hippocampal gamma oscillations *in vitro*. *J Neurosci* 2004; 24: 9127–9137.
69. Dugladze T, Schmitz D, Whittington MA, et al. Segregation of axonal and somatic activity during fast network oscillations. *Science* 2012; 336: 1458–1461.
70. Gloveli T, Dugladze T, Saha S, et al. Differential involvement of oriens/pyramidale interneurones in hippocampal network oscillations *in vitro*. *J Physiol* 2005; 562: 131–147.
71. Klausberger T, Magill PJ, Márton LF, et al. Brain-state- and cell-type-specific firing of hippocampal interneurons *in vivo*. *Nature* 2003; 421: 844–848.
72. Mann EO, Suckling JM, Hájos N, et al. Perisomatic feedback inhibition underlies cholinergically induced fast network oscillations in the rat hippocampus in vitro. *Neuron* 2005; 45: 105–117.
73. Oren I, Hájos N and Paulsen O. Identification of the current generator underlying cholinergically induced gamma frequency field potential oscillations in the hippocampal CA3 region. *J Physiol* 2010; 588: 785–797.
74. Attwell D and Gibb A. Neuroenergetics and the kinetic design of excitatory synapses. *Nat Rev Neurosci* 2005; 6: 841–849.
75. Attwell D and Laughlin SB. An energy budget for signaling in the grey matter of the brain. *J Cereb Blood Flow Metab* 2001; 21: 1133–1145.
76. Harris JJ, Jolivet R and Attwell D. Synaptic energy use and supply. *Neuron* 2012; 75: 762–777.
77. Howarth C, Gleeson P and Attwell D. Updated energy budgets for neural computation in the neocortex and cerebellum. *J Cereb Blood Flow Metab* 2012; 32: 1222–1232.
78. Liotta A, Rösner J, Huchzermeyer C, et al. Energy demand of synaptic transmission at the hippocampal Schaffer-collateral synapse. *J Cereb Blood Flow Metab* 2012; 32: 2076–2083.
79. Bucurenciu I, Bischofberger J and Jonas P. A small number of open Ca^{2+} channels trigger transmitter release

at a central GABAergic synapse. *Nat Neurosci* 2010; 13: 19–21.
80. Hefft S and Jonas P. Asynchronous GABA release generates long-lasting inhibition at a hippocampal interneuron-principal neuron synapse. *Nat Neurosci* 2005; 8: 1319–1328.
81. Rossignol E, Kruglikov I, van den Maagdenberg AMJM, et al. $Ca_V2.1$ ablation in cortical interneurons selectively impairs fast-spiking basket cells and causes generalized seizures. *Ann Neurol* 2013; 74: 209–222.
82. Zaitsev AV, Povysheva NV, Lewis DA, et al. P/Q-type, but not N-type, calcium channels mediate GABA release from fast-spiking interneurons to pyramidal cells in rat prefrontal cortex. *J Neurophysiol* 2007; 97: 3567–3573.
83. Li L, Bischofberger J and Jonas P. Differential gating and recruitment of P/Q-, N-, and R-type Ca^{2+} channels in hippocampal mossy fiber boutons. *J Neurosci* 2007; 27: 13420–13429.
84. Bucurenciu I, Kulik A, Schwaller B, et al. Nanodomain coupling between Ca^{2+} channels and Ca^{2+} sensors promotes fast and efficient transmitter release at a cortical GABAergic synapse. *Neuron* 2008; 57: 536–545.
85. Eggermann E, Bucurenciu I, Goswami SP, et al. Nanodomain coupling between Ca^{2+} channels and sensors of exocytosis at fast mammalian synapses. *Nat Rev Neurosci* 2012; 13: 7–21.
86. Cserép C, Pósfai B, Schwarcz AD, et al. Mitochondrial ultrastructure is coupled to cynaptic performance at axonal release sites. *eNeuro* 2018; 5.
87. Rangaraju V, Calloway N and Ryan TA. Activity-driven local ATP synthesis is required for synaptic function. *Cell* 2014; 156: 825–835.
88. Mably AJ and Colgin LL. Gamma oscillations in cognitive disorders. *Curr Opin Neurobiol* 2018; 52: 182–187.
89. Hollnagel JO, Elzoheiry S, Gorgas K, et al. Early alterations in hippocampal perisomatic GABAergic synapses and network oscillations in a mouse model of Alzheimer's disease amyloidosis. *PLoS One* 2019; 14: e0209228.
90. Barth AM and Mody I. Changes in hippocampal neuronal activity during and after unilateral selective hippocampal ischemia *in vivo*. *J Neurosci* 2011; 31: 851–860.